

Article

Partial Oxidation of *n*-Butane over a Sol-Gel Prepared Vanadium Phosphorous Oxide

Juan M. Salazar and Keith L. Hohn *

Department of Chemical Engineering, Kansas State University, 1016 Durland Hall, Manhattan, KS 66506, USA; E-Mail: jsalazar@ksu.edu

* Author to whom correspondence should be addressed; E-Mail: hohn@ksu.edu; Tel./Fax: +1-785-532-4315.

Received: 2 October 2012; in revised form: 5 December 2012 / Accepted: 8 January 2013 /

Published: 16 January 2013

Abstract: Vanadium phosphorous oxide (VPO) is traditionally manufactured from solid vanadium oxides by synthesizing $\text{VOHPO}_4 \cdot 0.5\text{H}_2\text{O}$ (the precursor) followed by *in situ* activation to produce $(\text{VO})_2\text{P}_2\text{O}_7$ (the active phase). This paper discusses an alternative synthesis method based on sol-gel techniques. Vanadium (V) triisopropoxide oxide was reacted with ortho-phosphoric acid in an aprotic solvent. The products were dried at high pressure in an autoclave with a controlled excess of solvent. This procedure produced a gel of VOPO_4 with interlayer entrapped molecules. The surface area of the obtained materials was between 50 and 120 m^2/g . Alcohol produced by the alkoxide hydrolysis reduced the vanadium during the drying step, thus VOPO_4 was converted to the precursor. This procedure yielded non-agglomerated platelets, which were dehydrated and evaluated in a butane-air mixture. Catalysts were significantly more selective than the traditionally prepared materials with similar intrinsic activity. It is suggested that the small crystallite size obtained increased their selectivity towards maleic anhydride.

Keywords: butane oxidation (partial); maleic anhydride; sol-gel process; supercritical drying; vanadium alkoxides; vpo catalysts

1. Introduction

The preparation of vanadyl pyrophosphate strongly influences its catalytic activity in the partial oxidation of butane to maleic anhydride [1,2]. The first step for this preparation is the synthesis of $\text{VOHPO}_4 \cdot 0.5\text{H}_2\text{O}$, referred to as the precursor in this paper. The type of reagents, the ratio of phosphorous to vanadium, the nature of the solvent and the conditions of the reduction step can control the characteristics of the precursor and thus the catalytic behavior of $(\text{VO})_2\text{P}_2\text{O}_7$ [1], which will be referred to as the active phase in this paper.

Several techniques have been applied to increase the activity of vanadium phosphorous oxide (VPO) catalysts and they are summarized by Hutchings [3] and Ballarini *et al.* [4]. Among them, we have focused on those that increase the surface area of either the precursor or the final active phase. It is interesting and important to notice that a high-surface-area precursor leads to an increase in the surface area of the active phase [3,5]. A classic approach is ball milling of the precursor. With this technique the surface area of the active phase was $40 \text{ m}^2/\text{g}$ compared to values of $3\text{--}11 \text{ m}^2/\text{g}$ obtained with the traditional preparations [5,6]. A more recent approach reached values of up to $41 \text{ m}^2/\text{g}$ when intercalation of primary alcohols and subsequent exfoliation were applied to $\text{VOPO}_4 \cdot 2\text{H}_2\text{O}$ (a vanadium (V) phase) [7,8]. Carreon *et al.* reported the synthesis of mesoporous VPO with surface areas as high as $250 \text{ m}^2/\text{g}$; however, this material was not stable during butane oxidation [3,4,9]. Carreon and Gulians obtained the active phase with a surface area of up to $44 \text{ m}^2/\text{g}$ by using polystyrene spheres as templates to generate macroporous materials [10]. Rownaghi and coworkers used a single-step process, high-pressure process where V_2O_5 was reduced by a series of primary alcohols at elevated temperatures [11]. They reported a precursor surface area of $23 \text{ m}^2/\text{g}$. The highest reported value of surface area has been $400 \text{ m}^2/\text{g}$, which was obtained by spreading the layers of $\text{VOPO}_4 \cdot 2\text{H}_2\text{O}$ apart with amine intercalation. These were denominated nickel pillared vanadyl phosphates [12].

Particle morphology and size are also important issues for the activity of the catalytic materials since small crystallites with exposure of the (100) plane are considered more selective [13,14]. Transformation from the precursor to the active phase is topotactic; the (001) plane on the former transforms into the (100) in the latter [15]. Thus, the morphology of the precursor plays an important role on the catalytic activity of the active phase [14]. In their work, Horowitz *et al.* reduced VOPO_4 to the precursor by secondary or primary alcohols. It was found that the type of alcohol dramatically influenced the morphology of the particles and consequently their catalytic activity [14]. The size of the crystallite has been demonstrated to affect the catalytic activity of VPO. Small crystallites of the precursor yielded small crystallites of the active phase and were reported as highly selective for the partial oxidation of butane to maleic anhydride [16–18]. Those small active crystallites are thought to form when the precursor crystallites break apart [19]. Therefore, synthetic routes that can be oriented to the manipulation of the precursor morphology, crystallite size and surface area are candidates to yield an improved catalyst.

Sol-gel methods have often been used to synthesize metal oxide catalysts and adsorbents due to their ability to regulate the composition and nanostructure of the final material during the earlier stages of synthesis [20]. The metal alkoxide method (MAM) is one of the most common sol-gel procedures. Metal alkoxides undergo hydrolysis and condensation to obtain colloidal gels whose structural

characteristics can be controlled. High surface area metal oxides are produced from this gel following an appropriate drying process [20]. Thus, the MAM is a likely candidate for synthesis of an improved precursor. The application of the MAM to vanadium phosphorous oxides has shown that reactions in aprotic solvents and in the absence of water lead to the formation of small and compact particles [21]. Other studies showed that the active phase could be synthesized through a sol-gel procedure and explored the application of colloidal and polymeric gelation to form membrane reactors [22]. Methods that involve the use of proton exchange resin are also reported in the synthesis of $\text{VOPO}_4 \cdot 2\text{H}_2\text{O}$ (a hydrated vanadium (V) phase) [23].

An important part of the sol-gel procedure, which for VPO has not been previously studied in any detail, is the procedure used to remove the solvent from the gel. This drying process can be carried out by evaporation or by the well known supercritical drying [24]. During the evaporation process the gel structure is affected by the high surface tension present in the liquid-gas interface. The very small pores of the gel are initially filled with liquid. As the liquid is vaporized, the walls of the pores can not resist the applied force and collapse, significantly damaging the gel structure, increasing the particle size and reducing the surface area [25]. This problem can be avoided if the evaporation process is carried out close to the critical point of the solvent where there is no surface tension [24,25]. The process is carried out in an autoclave and an appropriate excess of solvent is added to reach the critical point before the gel loses the solvent [24]. Several transformations of VPO can occur during this process. Different compositions, morphologies and subsequently different catalytic properties are reported as consequences of the high-pressure synthesis of VPO [26–28].

Several papers have evaluated the catalytic activity of precursors prepared from the exfoliation-reduction of $\text{VOPO}_4 \cdot 2\text{H}_2\text{O}$. We summarize some of the most relevant results from those works as follows. An exfoliated-reduced precursor in 1-butanol yielded an active phase with 3000 nm crystallite size that gave 53% selectivity to maleic anhydride at a conversion of 50% at 430 °C [7]. When 2-butanol was used as the exfoliating-reducing agent, the active phase with 800 nm crystallites was 75% selective at 50% conversion at 390 °C [16,17,19]. Finally, when the materials were exfoliated with a mixture of 2-butanol and ethanol, the active phase with 50 nm crystallites was 82% selective at 50% conversion at 390 °C [18].

High pressure and temperature preparations also yielded active catalysts for the partial oxidation of *n*-butane. $\text{VOPO}_4 \cdot 2\text{H}_2\text{O}$ was reduced with 1-octanol at 150 °C in an autoclave and the resulting material gave 50% selectivity at 39% conversion at 400 °C [27]. A precursor prepared by mixing V_2O_5 , H_3PO_4 , oxalic acid and water in an autoclave at 150 °C yielded an activated catalyst with 61% selectivity at 35% conversion at 400 °C [29]. Rownaghi and coworkers reported a maleic anhydride selectivity of 65% at a butane conversion of 53% from their catalyst synthesized by the reaction of V_2O_5 and 1-propanol at 373 K for 72 h [11].

The purpose of this study is to apply a sol-gel technique, namely the MAM, followed by near supercritical drying in an autoclave in order to increase the surface area of VPO. Characterization of the chemical composition and crystallite morphology of the products allow us to describe several possible influences of the synthesis and drying methodology on the catalytic activity.

2. Results and Discussion

2.1. Sol-Gel Synthesis in Tetrahydrofuran (THF)

The sol-gel procedure resulted in an immediate gelation process and an orange gel was observed. At this point, stirring using a magnetic stir bar was not possible due to the high viscosity of the solution. After three hours of aging, the mixture turned into a bright yellow slurry. The surface area of the slurry following atmospheric drying is 56 m²/g. The DRIFTS spectrum of this sample is shown in Figure 1 and the comparison with other reference materials is shown in Table 1. All of the vibrations of VOPO₄·2H₂O are present [23]. However, some of the bands assigned to this compound are missing, and some other weak ones (2993 cm⁻¹, 2893 cm⁻¹, 1460 cm⁻¹ and 1364 cm⁻¹) are not related to any of the vanadium phosphates. These bands are attributed to intercalated compounds as discussed below.

Figure 1. DRIFTS spectrum of vanadium phosphorous oxide (VPO) slurry in THF after drying in a stream of nitrogen.

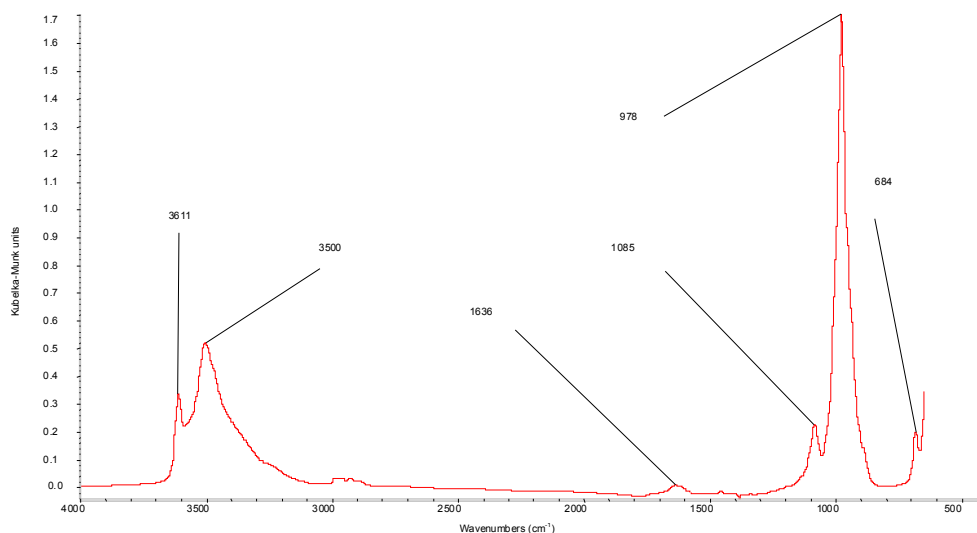


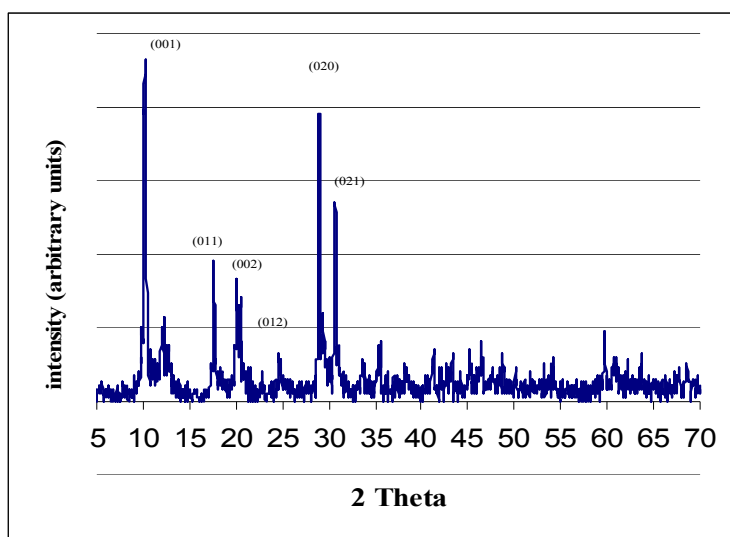
Table 1. DRIFTS and XRD analysis for Atmospheric Dried (AD) slurry.

DRIFTS wavenumbers in cm ⁻¹				XRD spacing in Å (relative intensity)		
Reference Compounds		This work	Assignment [21,38]	Reference Compounds [13]		This work
R1 ^a	THF	R2 ^b	AD	R3 ^c	R2 ^b	AD
		3620	3611			8.71 (100)
		3580	3500		7.45 (vS ^d)	7.32 (21.5)
2993	2993		2993			5.03 (40.9)
2893	2893		2893	4.43 (w ^g)		4.41 (35.5)
1464	1460		1460	3.57 (S ^e)		3.59 (11.8)
		1625	1636	3.07 (vS ^d)	3.1 (M ^e)	3.07 (83.9)
	1364		1346			2.91 (58.1)
		1088	1085		2.19 (w ^g)	2.18 (15.1)
		1000	978	1.9 (S ^e)		1.95 (12.9)
		913	911	1.83 (M ^f)		1.87 (14)
		685	684	1.56 (M ^f)	1.55 (S ^e)	1.55 (20.4)
				1.5 (M ^f)	1.52 (S ^e)	1.52 (13.4)
				1.43 (M ^f)	1.46 (M ^f)	1.46 (13.8)

^a 2-Propanol; ^b VOPO₄·2H₂O; ^c VOPO₄; ^d Very strong; ^e strong; ^f Medium; ^g Weak.

The X-ray diffraction pattern of AD, Figure 2, shows the presence of many of typical reflections of α -VOPO₄ as well as some of the reflections of VOPO₄·2H₂O [15], Table 1 compares the spacing and intensity of these referenced compounds with the AD. However, there are other very intense reflections at 8.71 Å, 5.03 Å and 2.91 Å that are not characteristic of any of the most well known VPO phases. These reflections are attributed to the intercalation of either solvent or isopropyl alcohol. Okuhara and coworkers recently explored the phenomena of exfoliation by means of intercalating alcohols into the layers of VOPO₄·2H₂O. The process was carried out for three hours at relatively low temperatures (30–70 °C) and the subsequent reduction of the exfoliated VPO by primary alcohols yielded the precursor [7,30]. Previous works employed alkylphosphonic acid that reacted with V₂O₅ to intercalate the corresponding alkyl groups and intercalated pyridine into VOPO₄·2H₂O by reflux [31,32].

Figure 2. XRD pattern of VPO slurry after drying in a stream of nitrogen.



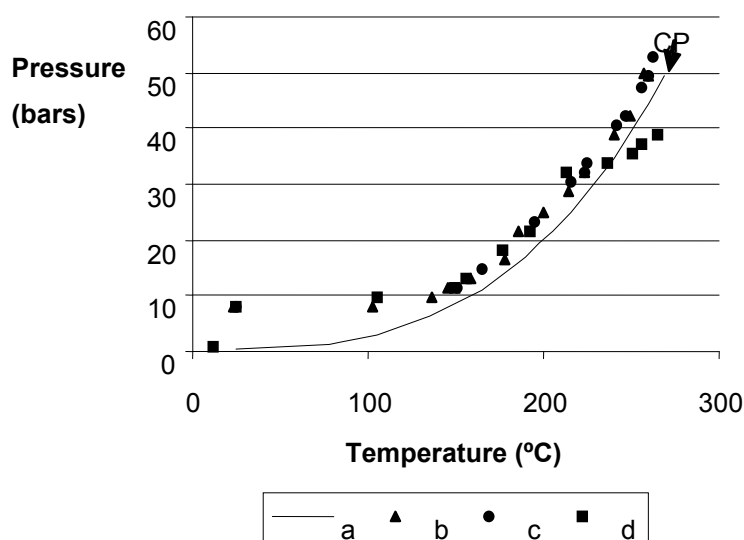
Thus, the DRIFTS and XRD patterns in Figure 1 and Figure 2 show VOPO₄ intercalated either with isopropyl alcohol or THF. This possibility is also supported by the presence of weak bands in the DRIFTS spectrum at 2993 cm⁻¹ and 2893 cm⁻¹ that correspond to C-H stretches of THF or isopropyl alcohol and the remaining weak bands that can be ascribed to these two compounds, Table 1. To substantiate that the sample was an intercalated VOPO₄, the XRD powder pattern was indexed to obtain the cell parameters. This calculation was done with CELREF software, version 3. A tetragonal cell symmetry was considered, which is the known symmetry of VOPO₄·2H₂O and other intercalated compounds. This calculation gave cell parameter values of $a = 6.158$ Å and $b = 8.868$ Å. The main (hkl) indices are shown in Figure 2. The hard sphere diameter for THF and 2-propanol was estimated according to the methodology reported by Misawa [33] and both are ~4.8 Å. This hard sphere diameter is approximately half of the b parameter for the powder pattern shown in Figure 2 (8.86 Å), which can be interpreted as an association of the intercalated molecules with each of the oxide layers that bound the intercalation space. This situation has been denominated as noninterdigitated intercalation, where double layers of the alcohol or THF are included into a VOPO₄ lamellar structure [34]. Even though THF was not considered as an exfoliation agent, THF or isopropyl alcohol could act as donor reagents,

intercalating the solid layers by donating electrons to the vanadium (V). At this time, we are unable to prove whether THF or isopropyl alcohol is the intercalated molecule.

2.2. Autoclave Drying

The pressure in the autoclave was measured for three levels of solvent (100 mL, 50 mL and 20 mL) as a function of temperature and is shown in Figure 3. For comparison, a theoretical curve of the liquid-vapor equilibrium of THF is also plotted [35]. When high and medium amount of solvent are added to the slurry before the drying step, the system develops a behavior similar to the vapor-liquid equilibrium of pure solvent and the liquid vaporizes very close to the critical point. In contrast, when a low amount of solvent is added, the liquid completely vaporizes and never reaches the critical point.

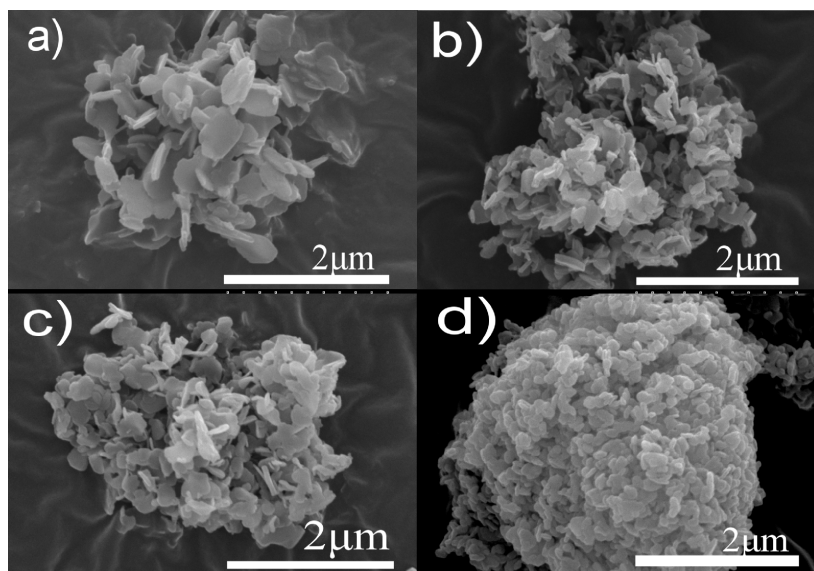
Figure 3. Pressure-temperature behavior during the autoclave drying compared with the vapor pressure of THF. (a) Vapor pressure of pure THF; (b) High amount of solvent (100 mL); (c) Medium amount of solvent (50 mL); (d) Low amount of solvent (20 mL). CP: Critical Point.



The morphology of the particles is strongly affected by the type of drying. Figure 4 shows that high pressure drying yields platelets while atmospheric pressure drying yields spherical particles (the atmospheric drying is in agreement with literature [36]). Among the high pressure treatments, the low amount of solvent (LS) produced larger particles and there is not a significant difference between the medium amount (MS) and the high amount (HS). The morphology of LS is typical of the precursor with phosphorous/vanadium ratios close to one [14]. Thus, in the autoclave drying, the amount of added solvent influences the conditions where it is completely vaporized [24] and influences the final size and morphology. An additional and interesting aspect is that the observed morphology of the particles after the drying step is very similar to those obtained by Okuhara and coworkers [7], but have a smaller particle size. Their claims include the formation of platelets of the reduced compounds with particle sizes of 500–6000 nm in length and 69–156 nm in thickness (calculated from surface area measurements). The reduced compounds shown in Figure 4 b,c are approximately 400 nm in length and the length of crystallites in Figure 4 a is 500 nm. For LS, MS and HS precursors the thickness of

crystallites was not calculated from surface area data due to the impurity (non-complete reduction) of samples.

Figure 4. SEM micrographs of VPO precursors prepared with the alkoxide method and (a) Autoclave drying, low amount of solvent (LS); (b) Autoclave drying, medium amount of solvent (MS); (c) Autoclave drying, high amount of solvent (HS); (d) AD.



2.3. Surface Area Measurements of Precursors

The surface areas of all autoclave-prepared precursors are shown in Table 2 and the influence of the amount of added solvent in this parameter is evident. The values are also higher than the results reported by Ennaciri for atmospheric pressure drying in air [36]. The analysis of variance for the experiment with the three levels of solvent results in the conclusion that there is no difference between MS and HS, but LS is different from the average HS and MS. The Bonfferoni t test was used to compare the means [37]. These results indicate that vaporization of the solvent during drying before the critical point leads to a dramatic loss of surface area.

Table 2. BET Surface areas for the products dried after adding the three amounts of solvent.

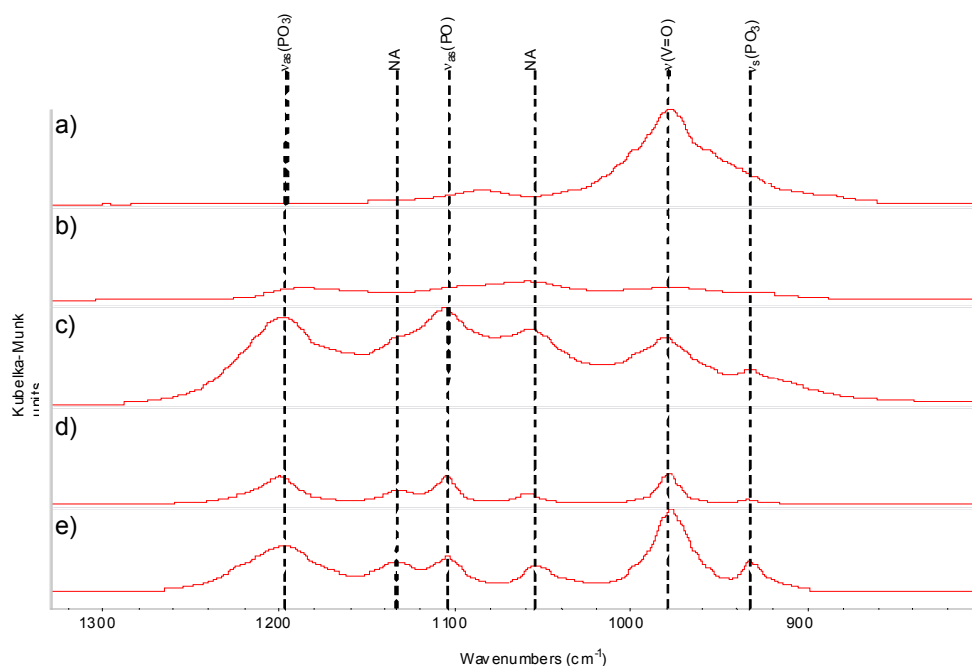
Precursor	Average Surface Area (m ² /g)
LS	65
MS	102
HS	121

2.4. DRIFTS and XRD Analysis

Infrared spectra and X-ray diffraction patterns were obtained for the materials dried with different amounts of solvent. These spectra, along with reference spectra, are shown in Figure 5a,e are DRIFTS fingerprints of VOPO₄ compounds shown in Figure 1 and the precursor respectively [23,38] Figure 5b–d show the evolution of spectra from VOPO₄ towards the precursor when the amount of added solvent is decreased. Bands at 1054 cm⁻¹, 977 cm⁻¹ and 1196 cm⁻¹ appear in Figure 5b, then 1104 cm⁻¹ and

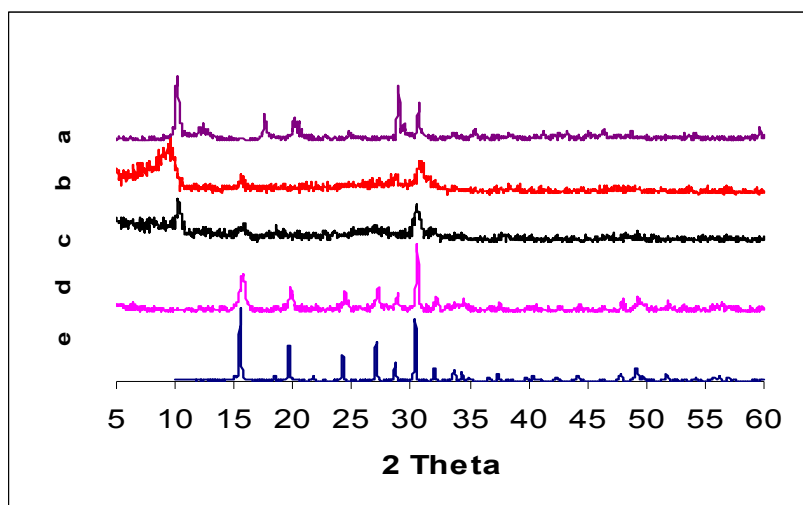
932 cm^{-1} are added in Figure 5c and finally 1133 cm^{-1} band shows up in Figure 5d to complete the six characteristic bands of the fingerprint spectra of the precursor. These spectra are very similar to those reported by Kamiya *et al.* for exfoliated-reduced $\text{VOPO}_4 \cdot 2\text{H}_2\text{O}$ [7]. The amount of added solvent in the three cases influences the chemical composition of the final materials. Similarly, Figure 6a,e are X-ray diffraction patterns of the VOPO_4 phase shown in Figure 2 and the precursor respectively [15]. In Figure 6b the reflections at 5.67 Å and 2.91 Å appear as the first sign of the presence of the hemihydrate. Figure 6c is mostly equal to the a), however the peak at 4.5 Å can be also observed and is associated with the main reflection of the hemihydrate (4.53 Å). Figure 6d is the closest pattern to Figure 6e since it contains additional reflections at 3.64 Å, 3.08 Å, 2.77 Å, 2.59 Å, 2.39 Å, 1.89 Å and 1.84 Å. Thus, the crystallography of the resultant materials evidences the transformation of the yellow slurry into a compound that can be identified as the precursor.

Figure 5. DRIFTS spectra of different VPO, (KM: Kubelka-Munk Units) (a) Slurry dried on nitrogen; (b) High amount of solvent; (c) Medium amount of solvent; (d) Low amount of solvent; (e) $\text{VOHPO}_4 \cdot 0.5\text{H}_2\text{O}$. NA: Non-assigned band.



These results show that in addition to the physical changes that occur during autoclave drying, chemical transformations also occur. Interestingly, while HS and MS had nearly the same surface area, they have quite different phase compositions. This suggests that the differences in surface area for these materials are not just due to differences in phase composition: the autoclave drying procedure has a substantial role in producing high surface-area vanadium phosphates.

Figure 6. XRD patterns of different VPO materials (a) Slurry dried on nitrogen; (b) High amount of solvent; (c) Medium amount of solvent; (d) Low amount of solvent; (e) $\text{VOHPO}_4 \cdot 0.5\text{H}_2\text{O}$.



2.5. Reduction Process inside the Autoclave

As discussed in the previous sections, when the material was dried inside the autoclave, chemical transformations occurred, which yielded products containing reduced-vanadium phases. The reduction process can be attributed to the alcohol generated as byproduct during the hydrolysis of the vanadium alkoxides. It is known that alcohols are good reducing agents to prepare the precursor [39]. Reduction of VOPO_4 with isopropyl alcohol and other alcohols has been reported to yield non-agglomerated particles with platelet crystalline morphology as a result of the reduction of VOPO_4 [14]; this is in agreement with the trend seen in Figure 4a–c. As more solvent was added to the slurry, the concentration of alcohol decreased and less reduced products were obtained. In contrast, low amount of added solvent resulted in more reduced phases. As measured through titration, the average oxidation state of the samples decreased with the amount of solvent.

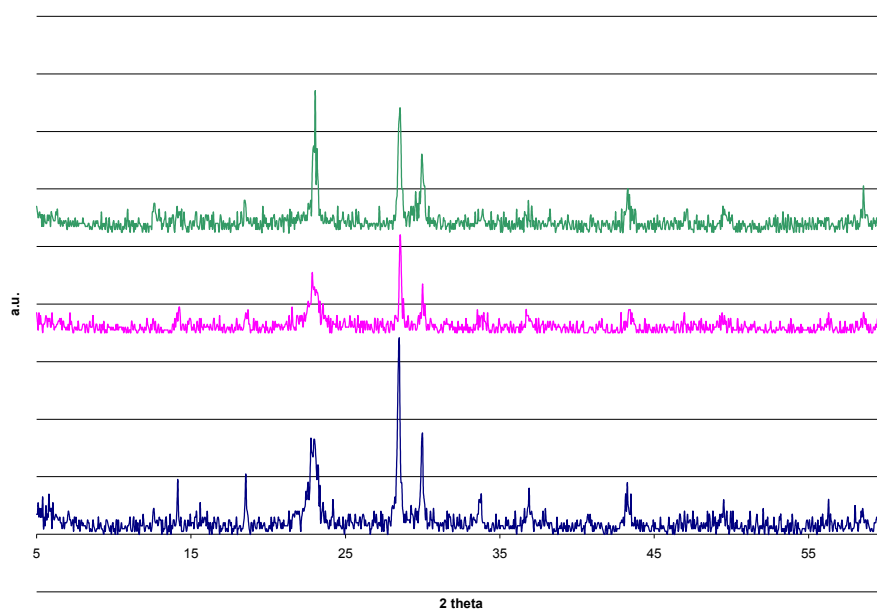
2.6. Catalytic Evaluation

The materials prepared on this study are compared with a control synthesized through the traditional methodology [14]. Conversion, selectivity and intrinsic activity are shown in Table 3. Traditionally prepared catalysts behaved in similar way as reported by Horowitz [14], even though their study activated the precursors under an oxidizing atmosphere and our activation (dehydration process) was under anaerobic conditions. The slight difference might be due to the formation of non-selective V^{3+} phases during activation under nitrogen; intercalated benzyl alcohol might have acted as a reducing agent [40]. Despite the possible formation of V^{3+} we chose this activation procedure to avoid the over-oxidation of the precursors with an aerobic atmosphere as suggested by the same authors [38]. Thus, this catalyst is an appropriate baseline to compare with the sol-gel prepared materials.

Table 3. Conversion, Selectivity and Intrinsic activities of traditionally and sol-gel prepared catalysts.

Treatment	Butane conversion	95% Confidence interval	Maleic anhydride selectivity	95% confidence interval	Intrinsic activity 10^{-5} mol MA/m ² /h
Traditional	37.4	(29.2, 41.7)	28.7	(22.6, 34.7)	2.11
Low solvent	31.1	(29.8, 39.7)	41.8	(35.7, 47.8)	1.13
Medium Solvent	20.6	(12.3, 29.0)	28.0	(22.0, 34.0)	1.8
High Solvent	28.4	(20.1, 36.6)	12.1	(6.1, 18.1)	1.17

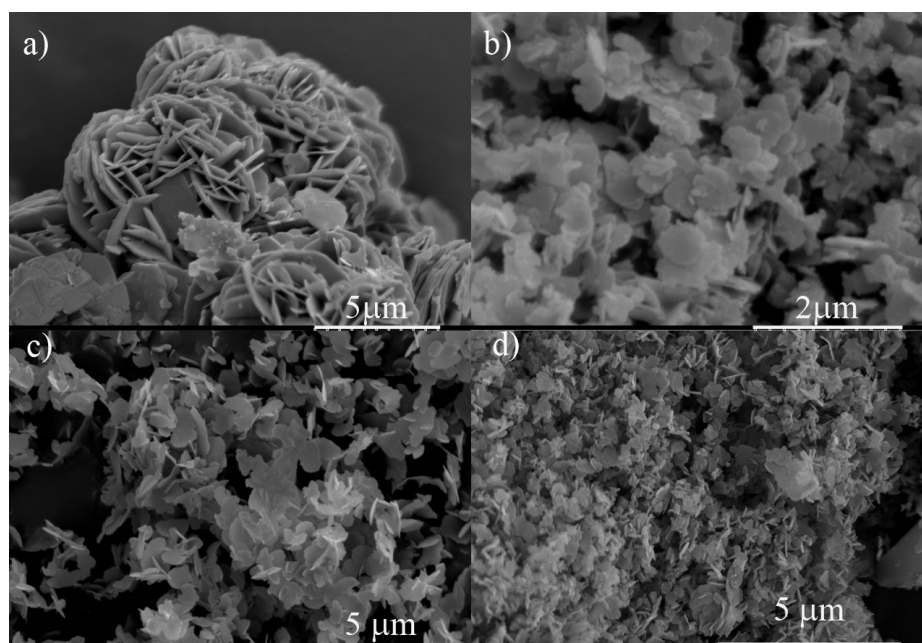
The conversion levels of the four catalysts were not significantly different, as seen by the overlapping of the confidence intervals in Table 3. Selectivity shows the tendency to increase when the amount of solvent used during the precursor's drying decreases. The confidence intervals for selectivity of traditional and low solvent treatment do not overlap meaning that the low solvent treatment is more selective. The confidence interval for the medium solvent treatment overlaps with the traditionally prepared material, suggesting similar selectivity, while the high solvent treatment has a lower selectivity than the traditional treatment. These results are attributed to the fact that the materials prepared with low amounts of the solvent have higher concentrations of the precursor and therefore, higher concentration of the active phase after activation. The activated catalysts are confirmed to be $(VO)_2P_2O_7$ by the XRD patterns in Figure 7 [15].

Figure 7. XRD patterns of activated catalysts from the precursors prepared with the three levels of extra solvent.

The scanning electron micrographs in Figure 8 illustrate the morphology of these materials. Small non agglomerated crystallites of about 600 nm in length are observed as activated catalysts from LS precursor. A similar shape but larger size, 1000 nm, is observed for active phase from MS and HS precursors. The crystallite thickness was estimated from both the Scherer's equation [29] and the

surface area [17]. The XRD-based calculation yielded 14 nm for those having 600 nm in length and 11 nm for those of 1000 nm; the estimation from the surface area measurements gave values of 4 and 7 nm respectively. This suggests that it cannot be assumed that the materials have a single morphology, so the surface area-based calculation is likely in error. Selective parts of the activated catalysts are suspected to be the very small particles present in Figure 8b produced by breaking down the corresponding precursor Figure 4a. The existence of the non selective low surface area domains is the reason for their low selectivity at the evaluated level of conversion (compared to those reported in the literature for small crystallites of the activated catalyst).

Figure 8. Scanning electron micrographs of activated catalysts from precursors prepared in (a) traditional synthetic route, atmospheric drying; (b) alkoxide method, autoclave drying, low solvent; (c) alkoxide method, autoclave drying, medium solvent and (d) alkoxide method, autoclave drying, high solvent.



3. Experimental Section

3.1. Sol-Gel Synthesis in THF

As a reference material for the catalytic evaluation, the precursor was prepared according to one of the traditional methods [14]. The procedure comprises the reduction of V_2O_5 with a mixture of alcohols (isobutyl and benzyl alcohol) and the addition of the phosphoric acid, 85% (Fisher). The sol-gel procedure was based on the reported methodology by Ennacciri *et al.* [30]. Two 1M solutions were prepared: (i) vanadium (V) triisopropoxide oxide (the alkoxide) (Alfa-Aesar) in tetrahydrofuran (THF) (Fisher) and (ii) orthophosphoric acid, anhydrous solid (Fluka), in THF (Fisher). Equal volumes (10 mL) of each solution were mixed. The phosphoric acid solution (ii) was added to the alkoxide solution (i) while stirring. The gel was aged for three hours and the final slurry was dried according to the procedure described below.

3.2. Drying Process

As a control procedure, the yellow slurry was dried under nitrogen at atmospheric pressure for four hours. This material will be referred to as AD. To dry the materials under high pressure, a reported procedure was followed [41]. The solvent and slurry was poured into a glass-lined 600-mL Parr reactor. The reactor was pressurized with nitrogen to 7.9 bars and heated from 25 °C to 265 °C at a rate of 1 °C/min. After ten minutes at the maximum temperature, the reactor was vented. In order to reach the critical point and avoid the collapse of the fragile gel, solvent was added before the slurry was dried in the autoclave [24]. To determine the influence of the amount of added solvent in the final product an experiment with a completely randomized design [37] was carried out with three levels or treatments: adding 20 mL, 50 mL or 100 mL (low, medium and high level, respectively) of THF. The resultant materials were referred to as LS, MS and HS respectively. Three replications were performed for each level.

3.3. Catalytic Evaluation

Precursors LS, MS and HS were evaluated as catalysts for the partial oxidation of butane to maleic anhydride. W/F (weight of catalysts per molar flow of n-butane) was adjusted to 60 g h mol⁻¹ for MS and HS (having bulk density up to 0.1 g/mL) and 150 g h mol⁻¹ for LS and traditionally prepared precursor (bulk density of 0.18 g/mL and above). This allowed us to keep gas hourly space velocities (GHSV) between 1700 h⁻¹ and 2200 h⁻¹. The precursors were initially treated under nitrogen from 298 K to 673 K and were kept at this temperature for 2 h. Next, a reacting mixture of 1.7% butane in air was flowed through the catalytic bed. The reaction was carried out for 72 h. The products were analyzed with gas chromatography employing a 5 Å molecular sieve and a Poropak QS column. The separated products were analyzed with a thermal conductivity detector (TCD) and a flame ionization detector (FID). The activated materials were referred to as CLS, CMS and CHS.

3.4. Characterization

Diffuse reflectance infrared Fourier transform spectroscopy (DRIFTS) was done with a Thermo Nicolet Nexus™ 670 FT-IR spectrophotometer equipped with a Smart Collector. The samples were diluted to 1–10 weight % in potassium bromide infrared grade (Acros). X-ray diffraction (XRD) was carried out with a Bruker axs D8 advance diffractometer that was set at 40 kV and 40 mA. Scans were from 5° to 70° (2θ) and with a step size of 0.05°. The diffractometer radiation was copper Kα (λ = 1.54 Å). The sample was put on the sample holder and exposed to the atmosphere at room temperature during the analysis. The scanning electron micrographs (SEM) were taken with a Hitachi S-3500N. The surface areas of the samples were determined by an Altamira instruments AMI-200 according to the BET model. The oxidation state of the vanadium in the samples was determined with the volumetric method reported in the literature [42].

4. Conclusions

A gelation process leads to production of hydrated and dehydrated VOPO₄, and some intercalated compounds, *i.e.*, compounds that have molecules of solvent or alcohol entrapped in the layers of the oxide. Drying these compounds at near supercritical conditions is a suitable procedure to produce improved materials, since it leads to the precursor with a well developed (001) plane, a platelet morphology and small crystallite size. The surface areas are dramatically affected by the amount of solvent added to the slurry, since it influences the final pressure of the autoclave. When the amount of solvent is doubled, the surface area is also doubled. This amount of solvent also affects the reduction process inside the autoclave. The composition of the obtained products changes from the intercalated VOPO₄ phase towards the precursor when the amount of solvent is cut in half. The sol-gel prepared precursors resulted in selective small crystallites of vanadyl pyrophosphate. The precursor dried with low amount of solvent (LS) yielded an activated catalyst (CLS) that is more selective than the traditionally prepared material at nearly the same conversion. However, CLS has a low intrinsic activity due to the low concentrations of precursor present in LS.

Conflict of Interest

The authors declare no conflict of interest.

References

1. Hodnett, B.K. Vanadium-Phosphorous Oxide Catalysts for the Selective Oxidation of C-4 Hydrocarbons to Maleic-Anhydride. *Catal. Rev. Sci. Eng.* **1985**, *27*, 373–424.
2. Centi, G.; Cavani, F.; and Trifiro, F. *Selective Oxidation by Heterogeneous Catalysis*; Kluwer Academic/Plenum Publishers: New York, NY, USA, 2001; p. 143.
3. Hutchings, G.J. Vanadium phosphate: A new look at the active components of catalysts for the oxidation of butane to maleic anhydride. *Mater. Chem.* **2004**, *14*, 3385–3395.
4. Ballarini, N.; Cavani, F.; Cortelli, C.; Ligi, S.; Pierelli, F.; Trifiro, F.; Fumagalli, C.; Mazzoni, G.; Monti, T. VPO catalyst for *n*-butane oxidation to maleic anhydride: A goal achieved, or a still open challenge? *Topics Catal.* **2006**, *38*, 147–156.
5. Hutchings, G.J.; Sananes, M.T.; Sajip, S.; Kiely, C.J.; Burrows, A.; Ellison, I.J.; Volta, J.C. Improved method of preparation of vanadium phosphate catalysts. *Catal. Today* **1997**, *33*, 161–171.
6. Higgins, R.; Hutchings, G.J. To Imperial Chemical Industries Limited. *US Patent 4 317 777*, 2 March 1982.
7. Kamiya, Y.; Ueki, S.; Hiyoshi, N.; Yamamoto, N.; Okuhara, T. Preparation of catalyst precursors for selective oxidation of *n*-butane by exfoliation-reduction of VOPO₄·2H₂O in primary alcohol. *Catal. Today* **2003**, *78*, 281–290.
8. Kamiya, Y.; Imai, H.; Okohura, T. Selective Oxidation of *n*-Butane over Highly Crystalline Vanadyl Pyrophosphate Catalyst Synthesized by Intercalation-exfoliation-reduction of Layered Vanadyl Phosphate Dihydrate. *J. Jpn. Petrol. Inst.* **2009**, *52*, 81–89.

9. Carreon, M.A.; Guliants, V.V.; Pierelli, F.; Cavani, F. Ordered mesostructured mixed metal oxides: microporous VPO phases for n-butane oxidation to maleic anhydride. *Cataly. Lett.* **2004**, *92*, 11–16.
10. Carreon, M.A.; Guliants, V.V. Macroporous vanadium phosphorous oxide phases displaying three-dimensional arrays of spherical voids. *Chem. Mater.* **2002**, *14*, 2670–2675.
11. Rownaghi, A.A.; Taufiq-Yup, Y.H. Novel Synthesis Technique for Preparation of Ultrahigh-Crystalline Vanadyl Pyrophosphate as a Highly Selective Catalyst for n-Butane Oxidation. *Ind. Eng. Chem. Res.* **2010**, *49*, 2135–2143.
12. Shpeizer, B.G.; Ouyang, X.; Heising, J.M.; Clearfield, A. Synthesis and crystal structure of a new vanadyl phosphate $[H-0.6(VO)_3(PO_4)_3(H_2O)_3] \cdot 4H(2)O$ and its conversion to porous products. *Chem. Mater.* **2001**, *13*, 2288–2296.
13. Centi, G.; Trifiro, F.; Ebner, J.R.; Franchetti, V.M. Mechanistic Aspects of Maleic-Anhydride Synthesis from C4-hydrocarbons over Phosphorus Vanadium-Oxide. *Chem. Rev.* **1988**, *88*, 55–80.
14. Horowitz, H.S.; Blackstone, C.M.; Sleight, A.W.; Teufer, G. V-P-O Catalysts for Oxidation of Butane to Maleic Anhydride—Influence of $(VO)_2H_4P_2O_9$ Precursor Morphology on Catalytic Properties. *Appl. Catal.* **1988**, *38*, 193–210.
15. Bordes, E. Crystallochemistry of V-P-O Phases and Application to Catalysis. *Catal. Today* **1987**, *1*, 499–526.
16. Kamiya, Y.; Hiyoshi, N.; Ryumon, N.; Okuhara, T. Microstructures of V-P-O catalysts derived from $VOHPO_4 \cdot 0.5H(2)O$ of different crystallite sizes. *J. Mol. Catal. A* **2004**, *220*, 103–112.
17. Hiyoshi, N.; Yamamoto, N.; Ryumon, N.; Kamiya, Y.; Okuhara, T. Selective oxidation of n-butane in the presence of vanadyl pyrophosphates synthesized by intercalation–exfoliation–reduction of layered $VOPO_4 \cdot 2H_2O$ in 2-butanol. *J. Catal.* **2004**, *221*, 225.
18. Kamiya, Y.; Ryumon, N.; Imai, H.; Okuhara, T. Nano-sized crystallites of vanadyl pyrophosphate as a highly selective catalyst for n-butane oxidation. *Catal. Lett.* **2006**, *111*, 159–163.
19. Ryumon, N.; Imai, H.; Kamiya, Y.; Okuhara, T. Effect of water vapor on the transformation of $VOHPO_4 \cdot 0.5H(2)O$ into $(VO)(2)P_2O_7$. *Appl. Catal. A* **2006**, *297*, 73–80.
20. Yan, C.; Sun, L.; Cheng, F. *Handbook of Nanophase and Nanostructured Materials*; Wang, Z.L., Li, Y., Zhang, Z., Eds.; Kluwer Academic/Plenum Publishers: New York, NY, USA, 2003; Volume 1, p. 72.
21. Ennaciri, S.A.; Bardoux, P. Solution Synthesis of Vanadium and Titanium Phosphates. *Mater. Sci. Forum* **1994**, *152–153*, 331–334.
22. Farrusseng, D.; Julbe, A.; Lopez, M.; Guizard, C. Investigation of sol-gel methods for the synthesis of VPO membrane materials adapted to the partial oxidation of n-butane. *Catal. Today* **2000**, *56*, 211–220.
23. R'kha, C.; Vandenborre, M.T.; Livage, J.; Prost, R.; Huard, E. Spectroscopic Study of Colloidal $VOPO_4 \cdot 2H_2O$. *J. Solid State Chem.* **1986**, *63*, 202–215.
24. Pierre, A.C. *Introduction to Sol-Gel Processing*; Kluwer Academic Publishers: Norwell, MA, USA, 1998; p. 242.
25. Teichner, S.J. In *Aerogels*; Fricke, J., Ed.; Springer-Verlag: Berlin, Germany, 1986; p. 22.
26. Griesel, L.; Bartley, J.K.; Wells, R.P.K.; Hutchings, G.J. Preparation of vanadium phosphate catalyst precursors using a high pressure method. *Catal. Today* **2005**, *99*, 131–136.

27. Dong, W.; Bartley, J.K.; Dummer, N.F.; Girgsdies, F.; Su, D.; Schloegl, R.; Volta, J.; Hutchings, G.J. Reaction of vanadium phosphates with alcohols at elevated temperature and pressure. *J. Mater. Chem.* **2005**, *15*, 3214–3220.
28. Griesel, L.; Bartley, J.K.; Wells, R.P.K.; Hutchings, G.J. Preparation of vanadium phosphate catalysts from $\text{VOPO}_4 \cdot 2\text{H}_2\text{O}$: Effect of $\text{VOPO}_4 \cdot 2\text{H}_2\text{O}$ preparation on catalyst preparation. *J. Mol. Catal. A* **2004**, *220*, 113–119.
29. Taufiq-Yap, Y.H.; Hasbi, A.R.M.; Hussein, M.Z.; Hutchings, G.J.; Bartley, J.; Dummer, N. Synthesis of vanadium phosphate catalysts by hydrothermal method for selective oxidation of *n*-butane to maleic anhydride. *Catal. Lett.* **2006**, *106*, 177–181.
30. Yamamoto, N.; Hiyoshi, N.; Okuhara, T. Thin-layered sheets of $\text{VOHPO}_4 \cdot 0.5\text{H}_2\text{O}$ prepared from $\text{VOPO}_4 \cdot 2\text{H}_2\text{O}$ by intercalation-exfoliation-reduction in alcohol. *Chem. Mater.* **2002**, *14*, 3882–3888.
31. Johnson, J.W.; Jacobson, A.J.; Brody, J.F.; Rich, S.M. Coordination Intercalation Reactions of the Layered Compounds VOPO_4 and VOASO_4 with Pyridine. *Inorg. Chem.* **1982**, *21*, 3820–3825.
32. Johnson, J.W.; Jacobson, A.J.; Brody, J.F.; Lewandowski, J.T. Layered Compounds with Alternating Organic and Inorganic Layers—Vandyl Organophosphonates. *Inorg. Chem.* **1984**, *23*, 3842–3844.
33. Misawa, M. Effective Diameter of Molecules and Liquid-gas Critical Point. *J. Chem. Phys.* **1990**, *93*, 8401–8402.
34. El Haskouri, J.; Cabrera, S.; Roca, M.; Alamo, J.; Beltran-Porter, A.; Beltran-Porter, D.; Marcos, M.D.; Amoros, P. Synthesis of a new mesostructured lamellar oxovanadium phosphate assembled through an (S+X-10) mechanism. *Inorg. Chem.* **1999**, *38*, 4243–4248.
35. Poling, B.E.; Prausnitz, J.M.; O'Connell, J.P. *The Properties of Gases and Liquids*; McGraw-Hill: New York, NY, USA, 2001; p. A-50.
36. Ennaciri, S.A.; Malka, K.; Louis, C.; Barboux, P.; R'kha, C.; Livage, J. Sol-gel synthesis and catalytic properties of vanadium phosphates Bulk materials. *Phosphorus Res. Bull.* **2000**, *11*, 87–93.
37. Kuehl, R.O. *Design of Experiments: Statistical Principles of Research Design and Analysis*; Brooks/Cole: Pacific Grove, CA, USA, 2000; p. 94.
38. Amoros, P.; Ibanez, R.; Martinez-Tamayo, E.; Beltran-Porter, A.; Beltran-Porter, D.; Villeneuve, G. New Vandyl Hydrogenphosphate Hydrates—Electronic-Spectra of the VO_2^+ Ion in the $\text{VO}(\text{H}_x\text{PO}_4)_x \cdot y\text{H}_2\text{O}$ System. *Mater. Res. Bull.* **1989**, *24*, 1347–1360.
39. Busca, G.; Cavani, F.; Centi, G.; Trifiro, F. Nature and mechanism of formation of vanadyl pyrophosphate—active phase in normal-butane selective oxidation. *J. Catal.* **1986**, *99*, 400–414.
40. Albonetti, S.; Cavani, F.; Ligi, S.; Pierelli, F.; Trifiro, F.; Ghelfi, F.; Mazzoni, G. The effect of glycols in the organic preparation of V/P mixed oxide, catalyst for the oxidation of *n*-butane to maleic anhydride. *Studies Surface Sci. Catal.* **2002**, *143*, 963–973.
41. Utamapanya, S.; Klabunde, K.J.; Schlup, J.R. Nanoscale metal-oxide particle clusters as chemical reagents—synthesis and properties of ultrahigh surface-area magnesium-hydroxide and magnesium-oxide. *Chem. Mater.* **1991**, *3*, 175–181.

42. Nakamura, M.; Kawai, K.; Fujiwara, Y. Structure and Activity of Vanadyl Phosphate Catalysts. *J. Catal.* **1974**, *34*, 345–355.

© 2013 by the authors; licensee MDPI, Basel, Switzerland. This article is an open access article distributed under the terms and conditions of the Creative Commons Attribution license (<http://creativecommons.org/licenses/by/3.0/>).